von KARMAN INSTITUTE
FOR FLUID DYNAMICS

INTERNAL NOTE 15

EXPERIMENTAL DATA FOR TANDEM CASCADE IN THE HIGH SUBSONIC REGION

by

C. SIEVERDING

RHODE-SAINT-GENESE, BELGIUM

September 1966

von KARMAN INSTITUTE FOR FLUID DYNAMICS

INTERNAL NOTE 15

EXPERIMENTAL DATA FOR TANDEM CASCADE IN THE HIGH SUBSONIC REGION

by

C. SIEVERDING

The research reported in this document was performed, under the supervision of Professor J. Chauvin, in partial fulfillment of the requirements for the diploma of the von Karman Institute, and sponsored as a whole by the Aerospace Research Laboratories, O.A.R. under Grant AF EOAR 65-65, through the European Office of Aerospace Research (OAR), USAF.

September 1966

TABLE OF CONTENTS

ACKNOWLEDGEMENTS

The author wishes to thank Professor Jacques Chauvin and Assistant Professor Franz Beugelmans for their guidance, interest and help in the presentation of this investigation. He would also like to thank Mr Michel Thiry, technical engineer and Mr Herman Joly who were both of invaluable help and assistance for the experimental part of this work.

BLANK PAGE

SUMMARY

The present work is the first part of studies on the use of the tandem cascade concept for application in the field of high turning angles. Two 1.64:1 scale models of a tandem cascade stator (ref. 2) - the second model was a slightly changed version of the original design - were tested in a cascade wind tunnel for free stream Mach numbers of M = .5 to .9 and incidence angles of I = -4° to +8°. Pressure measurements upstream; downstream and on the blade surfaces as well as schlieren pictures were taken. Application of back pressure was found to be necessary in order to get highest efficiencies and static pressure ratio. Side wall flaring or suction of the boundary layer at the side walls seem to be advisable for further testing.

The schlieren pictures show the strong influence of back pressure on the flow pattern inside the passage. The optimum values obtained for both tandem cascades are:
For M = .8

	tandem cascade I	tandem cascade II
turning angle θ	.54°	57.5°
total pressure loss ω	.145	.115
static pressure rise c_p	.41	.73

LIST OF SYMBOLS

C	chord
G	pitch
X/Y	coordinates parallel and normal to the cascade
X/G	displacement parallel to the cascade in per cent of the pitch (fig. 1b)
Y/C	displacement normal to the cascade in per cent of the chord (fig. 1b)
γ	stagger angle
σ	solidity
t	maximum thickness relative to chord
M	Mach number
P_o	total pressure
P_s	static pressure
Q	dynamic pressure
ω	total pressure loss coefficient
C_p	static pressaure rise coefficient
I	incidence angle
δ	deviation angle
Θ	air turning angle
β	flow angle
β'	blade angle
ϕ	blade turning angle
ρ	density
V	axial velocity
W	velocity

Suffixes and abbreviations

1,2	upstream, downstream
I/II	the first and the second blade row
E	single airfoil

G	influence of the other blades in the same row
J	influence of the other blade row
PS	pressure side (intrados)
SS	suction side (extrados)

Supercripts

-	average value

BLANK PAGE

1. INTRODUCTION

The development in turbomachinery leads more and more to highly loaded blades and therewith to high turning angles, because of the demand for few stages and therefore small weight, particularly in the field of high flight speeds and VTOL application. Turning angles exceeding the usual limits of a compressor design are encountered in the following cases:

1. Use of a big front fan for a jet engine
2. In lift engines
3. At the outlet of compressors with high subsonic axial Mach numbers.

The last problem is also given in our testfacility R-2 for a supersonic blunt trailing edge rotor. Outlet angles of 56° to 80° occur along the blade height and because of the demand for an axial outlet flow, turning angles of the same order have to be realized.

Two types of stators were considered for the solution

1. Blunt trailing edge concept
2. Tandem cascade concept.

The last concept was used by R. Kiock for the design of a stator (ref. 2) for the above mentioned rotor in R-2. For a better understanding and judgement of the operation of this concept an investigation of the mid-section of this tandem stator had to be carried out in the C-2 wind tunnel. The outlet angle of the flow at the mid-section of the rotor was measured to be 64 (ref. 1) which with a calculated optimum incidence angle of 10° leads to a stator blade angle of 54° (ref. 2).

2. CONCEPT AND THEORY OF A TANDEM CASCADE

While in accelerating cascades for turbines, high turning angles can be reached without too much difficulties due to the favourable pressure gradient, the strong adverse pressure gradient in a highly loaded compressor will easily lead to strong separations and therewith to high losses. In order to improve the flow pattern in a high turning passage, the passage is split into two rows so that one can achieve with each part of the cascade turning angles and loading coefficients which are within the usual limits. (fig. 1)

Unfortunately, all the experiments and theoretical investigations appearing in the literature are performed in the low subsonic region, so that the author could not compare his results with those available elsewhere.

A brief review of the technical literature concerning experimental and theoretical research on the tandem cascade is given below.

H. OHASHI (ref. 3) applies a variation of Schlichting's method for the calculation of the flow field. He takes into account the induced velocity from the other blade row by

$$W = W_E + W_G + W_J$$

Conclusion: agreement between experiment and theory for the first row fairly good, but very poor for the row II, due to the mutual interference of wake and boundary layer. The best agreement is found for the optimum configuration.

P. PAL (ref. 4) determines the flow field by the Martensen method. The calculation procedure is extended in order to take

more accurately into account the shape of the trailing edge of the first blade.
Conclusion: the pressure distributions are rather good as long as no separation occurs. The optimal configuration has proved to be that one where the axial displacement is zero and the circumferential displacement shows the configuration of slotted blades, that is, the second blade is placed close below the first one (see fig. Ia, Ib). Separation point and outlet angle have for both the theory and the experiment the same tendency. The losses for the optimal configuration can be approximately calculated and may be smaller than the losses without interference.

H. IHLENFELD (ref. 5) gives the criteria for the optimal displacement: the wake of the first blade must grow together with the suction side boundary layer at the trailing edge of the second cascade, that is, only one peak in the wake behind the cascade (fig. 2). Additional, both rows should have the same loading. Observing these c onditions a tandem cascade design may result in better aerodynamic coefficients than the sum of the two single rows.

H. LINNEMANN (ref. 6) investigated tandem cascades in a one stage fan. He found also the slotted blades to be the optimal configuration, for tandem stators even with a small axial overlap. At the optimal displacement the highest efficiency as well as the highest pressure rise coefficient will occur together.

W. RAILLY and M.E. EL-SARHA (ref. 7) extended the Ackeret method for the design of tandem cascades. They provide us with the only simple design method of this subject. This method shall be eminently suitable to solution on a digital computer.

The advantageous effect of a tandem cascade in the special configuration of slotted blades is due to:

1. a decrease in the suction peak at the leading edge of the second profile,
2. the injection of energy through the slot into the boundary layer on the suction side.

Both effects push the separation point towards the trailing edge.

Setting blade II above blade I is unfavourable because of separation on the suction side of blade I due to the pressure increase caused by the presence of the profile nose of blade II.

3. DESCRIPTION OF THE SET UP

The C-2 wind tunnel used for the tests is very similar to the one described in reference 9.

The tunnel is of the blowdown type, with high pressure air supply (60 m^3 at 40 kg/m). Wooden asymmetrical nozzles allow to operate at Mach numbers in the subsonic range as well as in the supersonic range. The side walls consist of plane perspex plates and allow visual survey of the flow. The arrangement of the outlet duct allows air turning angles by the cascade up to 90°. The downstream pressure can be varied by a throttling valve system.

The cascade as shown in fig. 1 represents the 1.64:1 scale model of the mid-section of the tandem stator, designed by R. Kiock (ref. 2). The two rows -each of them with six blades- are fixed in two disks which for different incidence angles can be rotated. The upper and lower porous wall in the test section can be adapted to the setting of the cascade. The main characteristics of the cascade are shown below:

	stator I	stator II
profile	double circular arc blades	double circular arc blades
max. thickness t/c	6%	6%
solidity σ	2	2
stagger angle γ	44°	20°
blade camber angle ϕ	19°30'	59°30'
displacement	Y/C = 0	X/G = .78

4. TEST PROGAM I

The following test program was performed with the above tandem cascade.

1. Measured data:

a. pressure distribution on the blade surfaces
b. static pressure increase
c. total pressure losses
d. deviation angle (turning angle)

2. Range of investigation

Test series I:	Mach number: .5 to .8	without backpressure
	incidence angle: -5° to 8°	medium backpressure
Test series II:	Mach number: .8 to .9	
	incidence angle: -1 to 5°	high back pressure

3. Schlieren pictures

Mach number: .7 to .9
Incidence angle: -1 to +5°.

5. TEST RESULTS AND DISCUSSION

5.1 Schlieren pictures

For a better understanding and judgement of the measurements we should look first at the schlieren pictures, which show us also the important influence of back pressure for high subsonic inlet Mach numbers.

Pictures 3 and 4 show that the inlet flow isnot quite uniform. The lower blades produce a slightly accelerated flow, combined with a slight change in the angle of attack, for the upper blades.

The inlet Mach number for the pictures in fig. 3 is kept constant ($M = .75$ for $i = -2°$) - total and static pressure are kept constant - while the outlet Mach number is varied by an increase of back pressure. Starting with very low back pressure, outlet pressure is equal to atmospheric pressure, the following flow and shock pattern are observed.

The acceleration of the flow due to the camber of the suction side as well as the acceleration around the leading edge to the pressure side leads the high subsonic free stream flow to supersonic velocity. This in turn will produce right behind the leading edge at the pressure side, an oblique shock. An oblique shock extended to the suction surface of the lower blade may be reflected. The flow, being still supersonic, will be further accelerated due to the divergent passage, as it is shown by weak Mach waves on the pictures. At the transition point from cascade I to cascade II several shock waves occur influencing each other. First an oblique shock will be produced at the trailing edge of the lower blade due to the angle between

blade surface and wake. This shock will interact near the leading edge of the upper blade II with a normal shock, generated by the presence of this blade, which will result in an oblique shock extending to the suction side of the lower blade II. Behind this shock exists a second oblique shock, almost parallel to the first one, attached to the leading edge of the upper blade because the flow behind the first oblique shock is still supersonic; or, the subsonic flow behind the normal shock, which has only a very short extension, is already again accelerated to supersonic velocity. The interaction of these shocks with the boundary layer on the suction side of the lower blade II causes a strong separation. The normal shock occuring behind the second oblique shock in the upper half of the passage cannot extend to the suction side because of this strong separation and will, therefore, end up in a bifurcated shock, called λ-shock. The left part of this λ-shock consists of compression waves generated by the angle between the blade surface and the sudden thickening of the boundary layer. Further downstream the boundary layer will increase in such a way that the rest of the cascade happens to be a convergent channel for the uniform flow that leads up to the outlet flow to normal shocks in this region. This shock pattern may result in an overall pressure decrease that is, acceleration, with very high losses. Unfortunately, no pressure distributions are available for this case. But the same tendency can be seen from fig. 10b (C_p-curve for M = .8).

Increasing back pressure will push the whole shock system out of the second cascade (pict. 3a to 3d). Finally, we observe the above mentioned oblique shock at the leading edge of cascade I and somewhere further downstream a normal shock; the position is of course a function of the strength of

the applied back pressure. Separation is observed on the suction side as well as on the pressure side.

It seems to be possible that there exist some shock configurations for which we may encounter higher losses with increasing back pressure. Let us for instance compare the following two cases:
1. a normal shock placed at the trailing edge of the first cascade and;
2. a normal shock which is placed very closely to the attachment point of the oblique shock on the suction surface in the first cascade.
The last one may cause separation with increasing losses, while the first one cannot affect the boundary layer due to the positive slot effect (see also discussion of the measured data).

The schlieren pictur series in fig. 4 is taken for a slight change in Mach number and incidence angle compared with those of fig. 3. The inlet Mach number could also not be kept quite constant, but the same influence of the back pressure on the development of the shock configuration is observed as in fig. 3. The central passage shows for the case of outlet at atmospheric pressure at the transition point of the two cascades two normal shocks, one right at the trailing edge of blade II, the second one at the leading edge of blade II. Back pressure pushes the normal shock, located at the trailing edge, further upstream, while the second one vanishes. For both cases an oblique shock exists at the leading edge of blade I.

The incidence angle for the 3 schlieren picture series in fig. 5 is increased to $+3.5^\circ$ while the Mach number varies as follows: M = .65, .8, .9. The outlet pressure is

constant (outlet pressure equal atmospheric pressure). As it can be seen from the tendency in the development of the pressure distributions (see chapter 5.2 and fig. 6, 7, 8), the local velocity will be much lower for I = 3.5° than for I = -2°. The acceleration around the leading edge to the pressure surface does not exist any more so that even for M = .8 no oblique shocks occur at the leading edges of the central passage. Further downstream supersonic velocities are reached due to a decrease of area. A normal shock located at about 50% of the passage length leads the flow again to subsonic velocity.

For M = .9, in fig. 5c, the flow picture is again more sophisticated. The shock system can be described with a normal shock right at the leading edge which develops down to the lower blade into an oblique shock. The blade surface reflects this shock and finally a normal shock leads to subsonic velocities. The last shock causes strong separations on the suction side. By a decrease of the flow area due to the presence of the second blade and the thick boundary layer, the flow is again accelerated to supersonic velocity at the leading edge of blade II as it is shown by weak shocks..

The performance of the slot seems to have a remarkable influence on the boundary layer development on the suction side of blade II.

The slot form can be divergent, convergent or of constant area. In the case of the investigated tandem cascade without overlap a slight convergent passage is established by the wake of the first blade and the suction surface of the second blade. The length of this passage is dependent on the length of the sharp limited zone of the wake which in turn is

influenced by the past history of the boundary layer of blade I. The flow coming from the pressure side in the first row will be accelerated in the slot and introduces high kinetic energy into the wake consisting almost alone of the boundary of the suction side. This jet stream tries always to resist a flow separation, which will be caused by a too high inverse pressure gradient or shock-boundary layer interaction. The energy of the jet stream is exhausted by friction onthe suction side and by mixing within the wake.

Some particular pattern of this passage flow are shown in picture 3 where the flow inside the channel is supersonic and presents a shock system very similar to that of a supersonic pipe flow. This shock pattern vanishes with increasing back pressure as well as the shock system in the second cascade. The influence of a convergent slot is dealt with in chapter 5.2.

5.2 Static pressure distributions

The static pressure distributions are plotted in figs 6, 7, 8. The pressures are made non-dimensional by dividing the difference of local and upstream static pressure by the dynamic head. The curve for 2° incidence angle represents the best performance.

Unfortunately, the pressure distributions do not correspond exactly to the schlieren pictures, but the experience gained from those may be a good help for the interpretation of those curves.

The curves presented include the following parameters:

incidence angle, Mach number and back pressure.

The incidence angle is responsible for the position of the maximal velocity. A variation of the incidence angle from -2 to +6 influences the position of the maximal velocity for M = .6 in both cascades only by a very little amount, while the maximal velocity for +2° shows a minimum for both cascades. For M = .8 the suction peak shifts with increasing incidence angle (-2° to 6°) towards the leading edge of the first cascade, while the maximum velocity has again a minimum for I = 2°.

The influence of the Mach number is small for I = 2°, but it increases with increasing deviation from the angle, particularly in the direction of negative incidences. Shocks occur for M = .8, for I=2° and I = 6°.

The best performance, that is, the lowest losses can be expected for an incidence angle of 2° because of the smooth behavior of the pressure development. Only, in this case the contribution to the overall static pressure rise is the same for both cascades. As it can be seen from fig. 6,7, the flow leaving cascade I may, for other incidences, even be accelerated. (M = .8). This was already known from the schlieren pictures.

The accleration on the suction surface II is mainly caused by the jet stream through the slot, but, on the other hand, also by the cascade flow being slightly inclined against the suction surface II. Using the same blades, a divergent slot could be established by changing the stagger angles. Such a variation would result in a deceleration of the velocity in the slot as well as in a smaller inclination of the main flow against the suction surface II. Both effects would diminish the suction peak in the second row.

It should be noticed that the optimum incidence angle of the actual stator was calculated to I = 10°, while in the cascade the optimum incidence angle was found to be I = 2°. Knowing now how strong the influence of a variation of the incidence angle on the performance of the cascade is, particularly for high subsonic Mach numbers, we have to expect results in the actual stator which differ a great deal from the optimal results measured in the wind tunnel.

5.3 Total pressure losses

Fig.9a and 9b present the curve for the total loss coefficient = $\frac{P_{02}-P_{01}}{Q_I}$. Fig. 9a shows ω as a function of the incidence angle with the free stream Mach number M_I as parameter for the case of applied back pressure; fig. 9b shows a similar graph for the case of outlet at atmospheric pressure. The following statements can be made:

a. for an outlet at atmospheric pressure

1. All curves have about the same optimal incidence angle of +2°. This is against the experience, meaning that the optimal incidence angle for blades with a sharp leading edge increases with increasing Mach number.
2. The minimum losses are measured to
   ω = .11 to .12 for M = .5, .6, .7 and to
   ω = .13 for M = .8
3. The range of operation reaches
   for M = .5, .6 from -8° to +6.5°
   for M = .7 from -1,5° to +6.5°
   for M = .8 from - .5° to +5.5°
   The operation range is limited by loss values being twice as high as the minimum losses.

b. for back pressure applied

1. The optimum incidence at 2.5° is a little bit higher than in the case without back pressure; however, the lowest losses occur for all inlet velocities again at the same incidence angle.
2. The minimum losses for M = .5, .6, .7 are about 1 point lower than the values above, but for M = .8 losses are recorded being two points higher than the above. An explanation has already been attempted in chapter 5.1. Measurements taken for M = .9 come out with ω_{min} = .20.
3. The operation range is limited

for M = .5, .6	from	-6.5°	to	+7.5°
for M = .7	from	-2°	to	+6°
for M = .8	from	-1.5°	to	+6°
for M = .9	from	-2°	to	+8°

The definition of the operating range is not very useful for high Mach numbers, because operation in this regime leads to too high losses.

From these statements the following conclusions can be drawn:

1. From the point of view of losses, application of back pressure does not improve the performance in each case.
2. Considering the range of operation the advantage of the application is limited to high free stream Mach numbers.
3. The main advantage of applying back pressure for low Mach numbers M = .5, .6 lies on the relative decrease of losses for higher positive incidence angles, that is, for increasing turning angles. The improvement for I = +6° is about 6 points, for optimum incidence only one point.

5.4 Static pressure increase

Figs. 10a and 10b show the overall static pressure

rise, expressed as $C_p = \frac{P_{S2}-P_{SI}}{Q_I}$, as a function of the incidence angle for different Mach numbers and back pressures. The superiority of the application of back pressure can clearly be seen.

The following statements can be made:

a. about the case of an outlet at atmospheric pressure, fig.10b
   1. The optimum pressure rise comes out to be at the same incidence angle as the lowest losses.
   2. High Mach numbers M = .7, .8 yield already for I = -2°, respectively I = +.5°, negative C_p values; that is, the cascade acts as a turbine cascade. This possibility was already shown by the schlieren pictures fig. 3 and by the pressure distributions fig. 6.
   3. The optimal point increases with decreasing Mach number from C_p = .37 for M = .8 to C_p = .40 for M = .5, .6.
   4. The range of operation increase with decreasing Mach number.

b. about the case of back pressure applied
   1. The optimum incidence angle shifts from I = 2° for M = .7, .8 (test series 1) to I = 1 for M = .5, .6. The deviation from the optimum incidence of the loss curves is small and results only in a small variation of the C_p values.
   2. The range as well as the pressure increase itself has been improved a great deal, particularly for high Mach numbers and incidence angles away from the optimum one.
   3. The optimum values differ only a little amount from each other, C_p = .40 for all Mach numbers.
   4. The additional test series II with a further increase of back pressure yields a much higher pressure rise with maximum values for M = .8 of C_p = .55 and for M = .9

with C_p = .63. The optimum incidence is here measured to I = 0°. These values seem to be rather high, even if we consider that, by pushing the normal shock (see schlieren pictures) in the first cascade through an increase of back pressure further towards the leading edge, higher C_p values than those of series 1 can be expected.

Summarizing these statements, we can finally say that the application of back pressure is to be recommended, because:

1. the agreement of optimal incidence angle of the ω- and C_p-curves is still very good,
2. back pressure extends the operating range for all Mach numbers and
3. increases the overall static pressure rise, particularly for high Mach numbers for negative incidences.

The advantageous effect of increasing back pressure has to be fully utilized.

A comparison of the static pressure rise measured by the probe and that one which has to be expected by the pressure distribution on the blade surfaces gives in general good agreement (see fig. 10 a,b series 1 and figs. 6, 7, 8). Slight deviations observed do not give any exact tendencies.

5.5 Deviation angle and air turning angle

Figs. 11 a,b give the deviation angle as a function of the inlet angle.

The results for the case of an outlet at atmospheric pressure confirm the experiences that the deviation angle in first approximation can be taken as independent on the inlet angle, that is, of course, only true within a certain range of incidence angles. It is also shown that the incidence angle is almost independent on the Mach number as it can be seen from the following figures:

for I = -2°	is	$\delta = 9°$	for M = .5, .6, .7
for I = +6°	is	$\delta = 9.1°$	for M = .5
	and	$\delta = 8.6°$	for M = .6, .7, .8

A completely different picture is shown by the graphs for the case of back pressure applied. Within a range of I = -2° to I = +6° the deviation angle varies for all Mach numbers of about 4°, the maximum deviation being at the optimum incidence angle for the losses and the overall static pressure increase. From I = 2° with $\delta = 12°$ for M = .5, .6, .7 and $\delta = 11°$ for M = .8, the curves come down to $\delta = 8°$ for M = .5, .6, .7 for M = .8.

The values for the test series II with back pressure further increased, show about $\delta = 12°$ = constant for M = .8 and for M = .9 in the optimum point a value close to that of M = .8 of series I.

These results applied to the turning angle, give the following conclusions (see figs. 12 a,b).

1. The turning angles for all measured Mach numbers for an outlet at atmosoheric pressure increase at the same rate as the incidence angles and they can be presented by a single curve.
2. The turning angles for applied back pressure are almost constant up to 2° incidence, except for series II. Above 2°

the turning angles increase even at a higher rate than in the case without back pressure and end up for I=6° with θ = 62° respectively 61° for M = .5, .6, .7 and M = .8, compared with θ = 61° for the first case.

5.6 Axial velocity ratio

Figs 13 a,b present the mass flow ratio $A = \frac{\rho_2 \cdot V_2}{\rho_1 \cdot V_1}$ where V_2 and V_1 are the axial velocities downstream and upstream. For the case of a two dimensional flow this ratio should be A = 1. Disregarding the error in the measuring system, a deviation from A = 1 is due to the disturbance of the two dimensionality of the flow, which can be explained:
1. by some leaks in the test section, as for instance the slot for the probe which cannot be air tight closed;
2. by boundary layer separations at the side walls. The latter one giving the main contribution to a value A > 1. Assuming that a change in the density ratio ρ_2/ρ_1 to this side wall boundary layer effect is small, A > 1 is mainly a variation in the axial velocity ratio; therefore, the curves in fig. 13 may be regarded as a change in axial velocity ratio in function of the incidence angle.

In general, the curves in fig. 13 show a tendency for A to increase with increasing incidence angle, because higher incidences give higher turning angles and therewith higher deceleration and separation at the side walls, leading to an acceleration of the outlet flow in the measuring plane. We witness again the favourable influence of back pressure on the flow behavior, however, this influence on A is limited. For the optimum incidence I = 2°, an average value of A = 1.25 for the different Mach numbers was measured for the case of

back pressure applied as well as for the case without back pressure. For the other incidences A is in general a little bit lower for back pressure applied.

The flow separation at the side walls has, however, a favourable influence on the flow in the measuring plane. W. Heilmann (ref. 8) made some investigations on this subject. A suction system enabled him to diminish the ratio A to the value 1, corresponding to a two dimensional flow, or even lower. He found out that the total pressure losses and the deviation angle increase very fast with a decreasing velocity ratio. The results can then be expected to be slightly optimistic.

6. TEST PROGRAM II

The results of the investigation of tandem cascade I, brought up the question of whether it would be possible to increase the turning angle with this cascade by increasing the stagger angle of blade I and how the flow behavior of this changed version would be. A simple calculation shows that

$$\beta_{2_I} - \beta_{1_{II}} = 16°$$

For this reason the attempt was made to increase the stagger angle of blade row I from 44° to 54°. At the same time the axial displacement of the two stators was slightly changed to:

$$Y/C = -0.04 \qquad X/C = 0,87$$

The measuring program for the new tandem cascade II was about the same as for tandem cascade I except that no schlieren pictures were taken. Some tests showed that the range of incidence angles would have an upper limit of I = 2° because for higher incidence angles the downstream uniformity could no longer be preserved.

7. TEST RESULTS OF TANDEM CASCADE II AND DISCUSSION

According to the higher stagger angle and therewith to a minimized throat area sonic conditions will be reached much earlier than for cascade I. This in turn already indicates a higher influence of back pressure application. The main discussion will therefore be restricted to this problem.

7.1 Static pressure distribution

Static pressure distributions are presented only for Mach number M =.8, and incidence angle I = 1°, and several back pressures.

The picture in fig. 14 gives an idea about the high influence of back pressure application and shows themain difference between both versions of the tandem cascade.

a. The position of the maximal velocity in the stator I is reached for all back pressures applied at about 50% of the chord downstream. Increasing back pressure decreases constantly the peak velocity.

b. Stator II shows a completely different and rather unusual picture. The main difference relies in a negative lift between 35% and 70% of the chord downstream. The following explanation was found:the slot corresponding to the increased stagger angle γ_I is no longer convergent but almost of constant area. Furthermore, the flow coming from the suction surface of blade I is no longer inclined against the suction surface of blade II. Both effects result in a further continuous deceleration of the flow or even higher because of the higher camber angle of blade II until the boundary layer can no longer resist the adverse pressure gradient.

On the other hand, the flow is now inclined against the pressure surface of blade II leading first to an acceleration of the flow. Further downstream deceleration occurs again due to the area increase.
The extremely strong deceleration on the suction side and the acceleration in the first part of the pressure side result in the above mentionned negative lift.

7.2 Total pressure loss and static pressure increase

Figures 15 a,b,c show us an impressive drop in the loss curve for increasing back pressure. Optimum values of $\omega = .22$ for the lowest back pressure come down to $\omega = .12$ for the highest back pressure.

A similar picture is shown in the figs 16 a,b,c, which present the static pressure rise as a function of the incidence angle with the back pressure as parameter. Highest values of $C_p = .75$ are recorded, that is an increase of 20 to 25% between the lowest and the highest back pressure. The influence of Mach number is not very strong. The optimum values are measured for the losses as well as for the static pressure increase for an incidence angle of -1° to -2°.

PLotting now the losses $\bar{\omega}$ versus the static pressure increase $\bar{C}_p$, we make the following interesting statements:

1. $\bar{\omega}$, as a function of $\bar{C}_p$ for one Mach number, can be presented by a single curve.
2. Values for incidence angles between -5° and 2° fit this single curve very well. Restrictions must be made for low $\bar{C}_p$ values where the points have a rather strong scatter. This means for the longest and most important part of the curve, the range of operation covers at least a field of

about 7° incidence angle.

3. In the region from $\bar{\omega}$ = .20 down to the lowest values the curves for all three Mach numbers measured are almost identical, while the curves show an increasing divergence for higher losses. The curve for M = .6 is a straight line but shows in this part for M = .8 a parabolic development.
4. The dependence of ω on C_p as it is shown by these graphs was also found in other cascade tests in supersonic flow and in transonic flow as well. (ref.10). A comparison with these gives a good agreement in the characteristic symptoms.

7.3 Deviation angle and air turning angle

Figs. 18 a,b,c present the deviation angle as a function of the incidence angle. The optimum values lie for all Mach numbers and back pressures at about I = 0. The best results show again only a very small difference, δ = 14 to 15°. Increasing values are recorded for incidence angles deviating from the optimum one. For these graphs and all the others, the curves with the lowest back pressure show an unsteady behavior. This makes it difficult to give a more detailed discussion of these datas.

The calculation of the air turning angles gives us finally the information of whether the purpose of the tests - to get a higher turning angle with reasonable losses - was reached or not. Although restrictions must be made because of the rather small range of datas available for the turning angles, it can be stated:

1. The development of the curves are different for both cascades: steady increase of θ with I for tandem cascade I, optimum value of θ for tandem cascade II.

2. The turning angle for the point of lowest losses could be raised only by 4° from 53° to 54° for tandem cascade I to 57° to 58° for tandem cascade II (The tests performed with outlet at atmospheric pressure are not taken into account for this comparison).

The improvement in the turning angle is in fact less than what we would expect from the results obtained for the static pressure increase and the total pressure losses. It is rather difficult to find an explanation for this phenomena.

8. CONCLUSIONS

1. The investigated tandem cascades bring out high turning angles combined with reasonable total pressure losses and considerable static pressure increase.

2. The minimum total pressure loss and the maximum static pressure increase occur about the same incidence angle.

3. The application of back pressure is found to be advantageous and has to be fully utilized. A comparison of tandem cascade I and tandem cascade II makes it probable that a further increase of the back pressure could improve the performance of tandem cascade II.

4. The slot dimensions are in both cases not yet optimal and they play an important role for the flow behavior on the blade surfaces.

5. The stagger angle γ_I for tandem cascade II was choosen too high. An increase of 5° only instead of 10° will probably be the correct value.

6. Strong flow separations at the side wall make the application of side wall flaring advisable.

REFERENCES

1. BREUGELMANS, F. & KIOCK, R.: Investigation of a one stage axial flow supersonic compressor.
V.K.I. IN 12, part II

2. KIOCK, R.: Stator design for the high speed compressor R-32.
VKI Project Report 65-134

3. OHASHI, H.: Theory of mutual interference in tandem compressor cascades.
Bulletin of the Japan Soc. Mech. Eng.; vol. 7, n° 25, p. 71.

4. PAL, P.: Untersuchungen über den Interferenzeinfluss bei Strömungen durch Tandem-Schaufelgittern.
Ing. Archiv 34, S. 173; 1965.

5. IHLENFELD, H.: Strömungsvorgänge an geraden stark verzögernden Spaltflügelgittern.
Mitteilung aus dem Inst. für angew. Strömungslehre der TU Dresden.

6. LINNEMANN, H.: Untersuchungen eines einstufigen Axialgebläses mit Tandemgittern.
Konstruktion, Heft 4, S. 128, 1964.

7. RAILLEY, W. & EL-SARHA, M.F.: Ackeret method for the design of tandem cascades.
Engineer, London 1965, 219, June 25th, 1085.

8. HEILMANN, W.: Mitteilungen aus der deutschen Versuchsanstalt für Luft- und Raumfahrt.

9. HERMANN, P.: Further investigations of a blunt trailing edge cascade in the S-3 supersonic wind tunnel. VKI [illegible] 9.

10. BREUGELMANS, F., SIEVERDING, C.: Cascade data for high camber blunt trailing edge blades. VKI IN 17 (in preparation).

LIST OF FIGURES

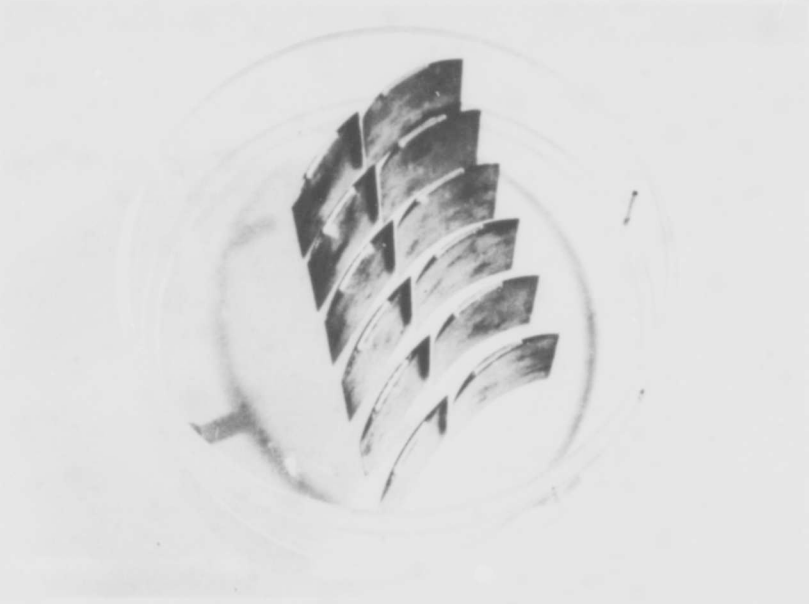

Fig 1a TANDEM CASCADE I

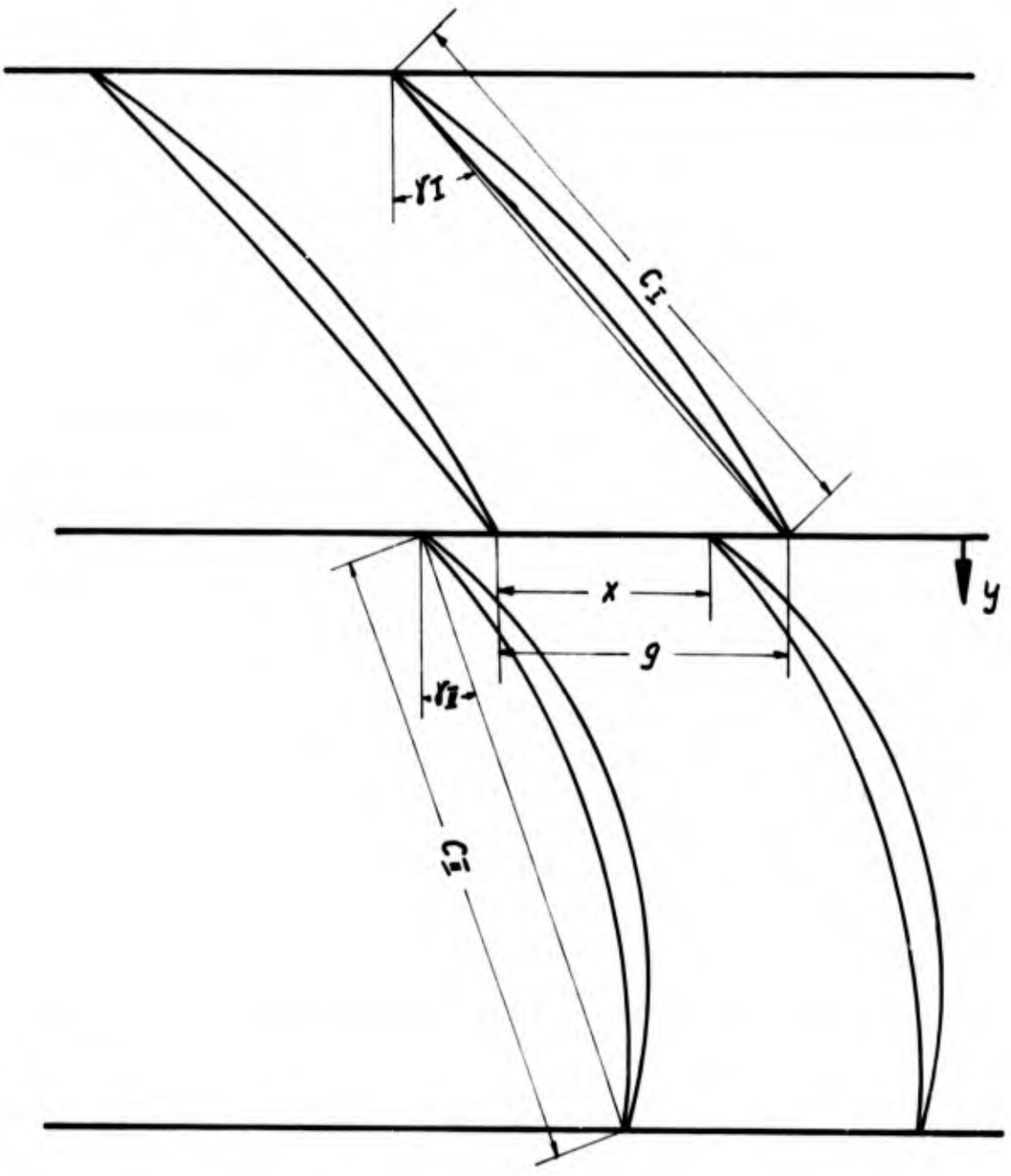

fig: 1b tandem cascade I

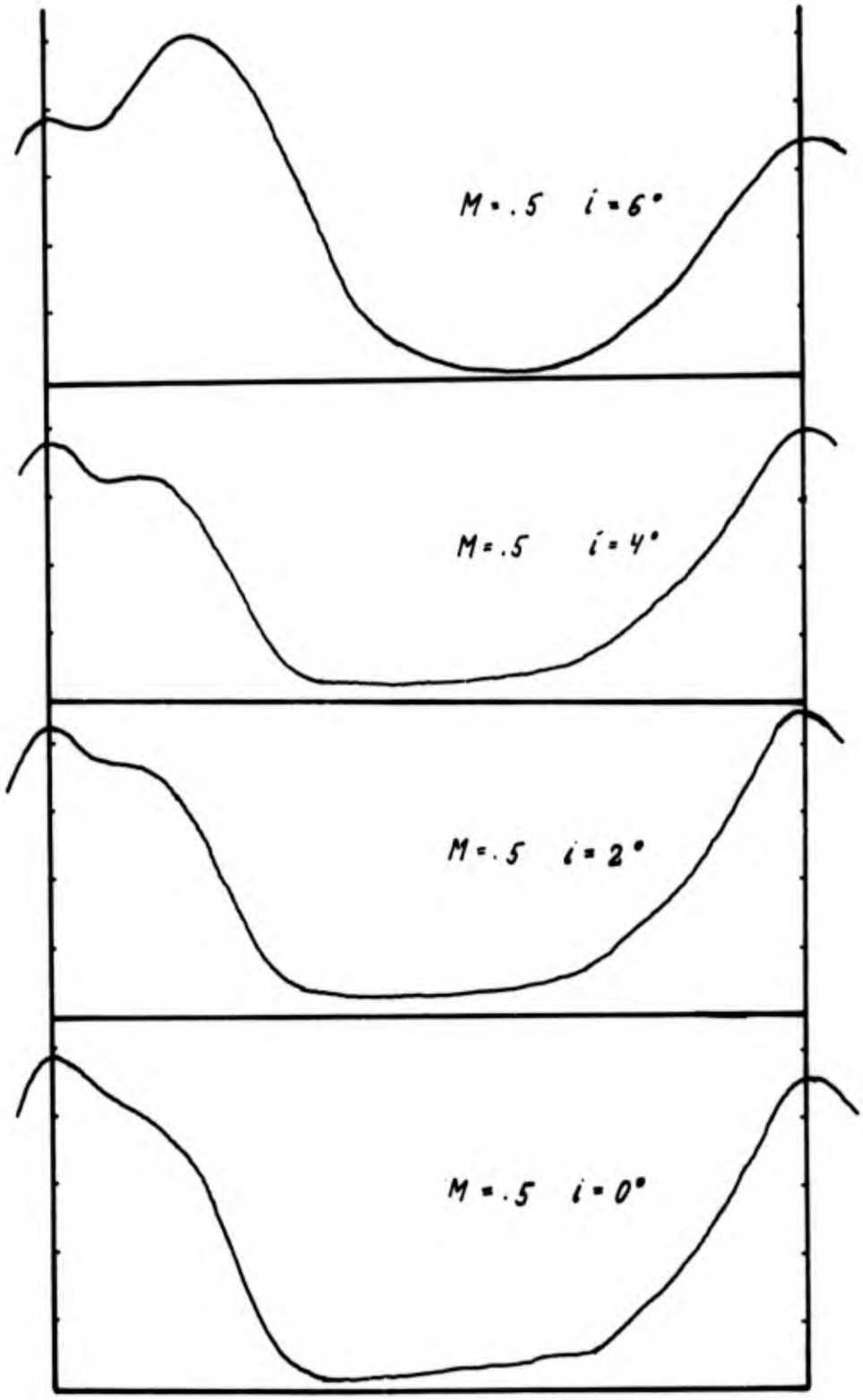

fig:2 loss distribution behind tandem cascade I
(backpressure applied)

fig. 3a

3b

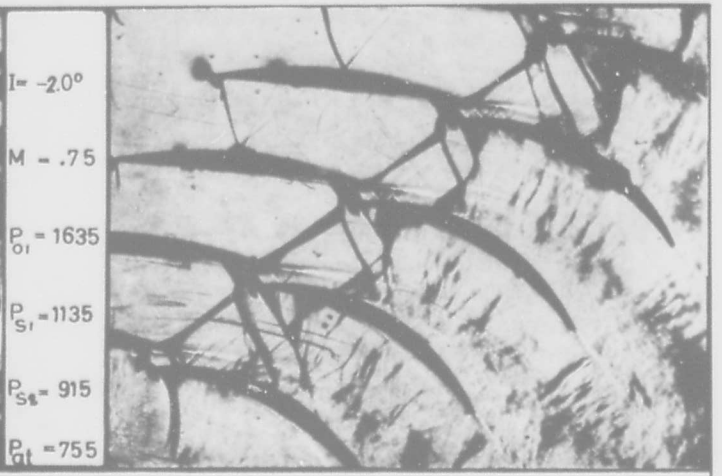

3c

3d

tandem cascade I

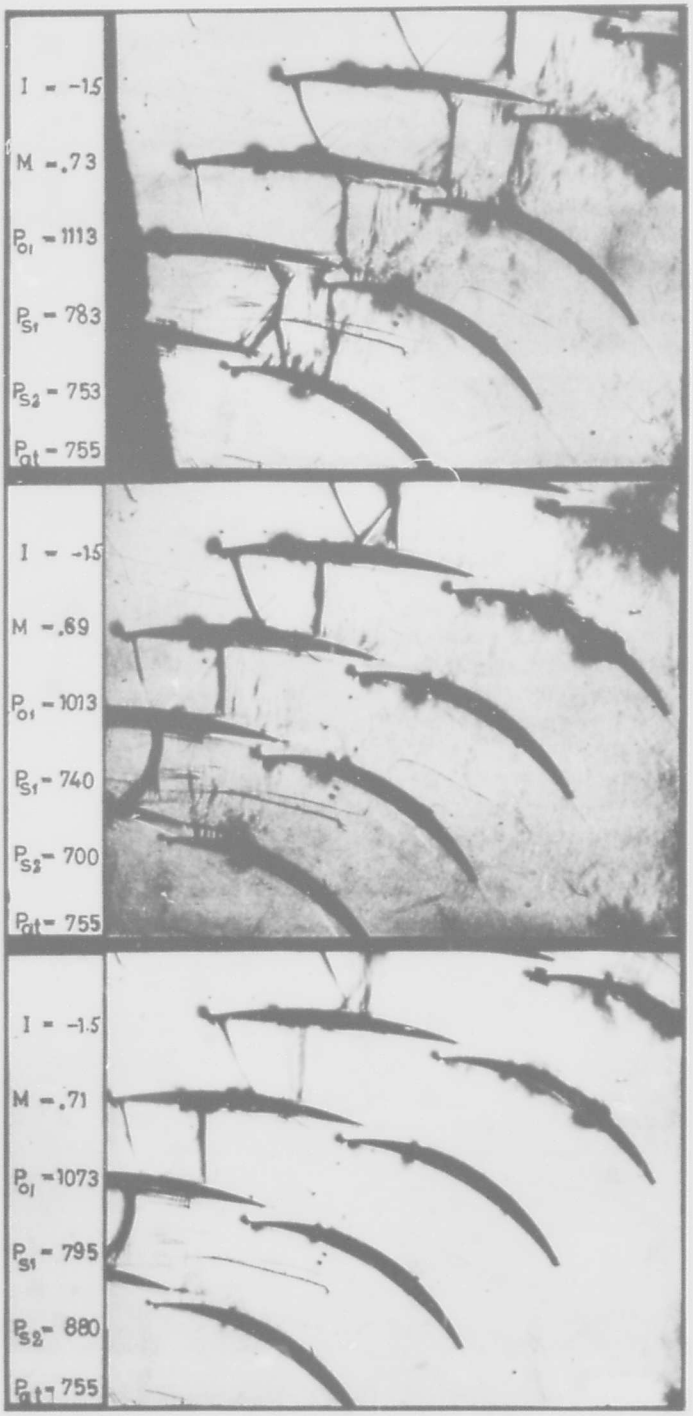

fig. 4a

4b

4c

tandem cascade I

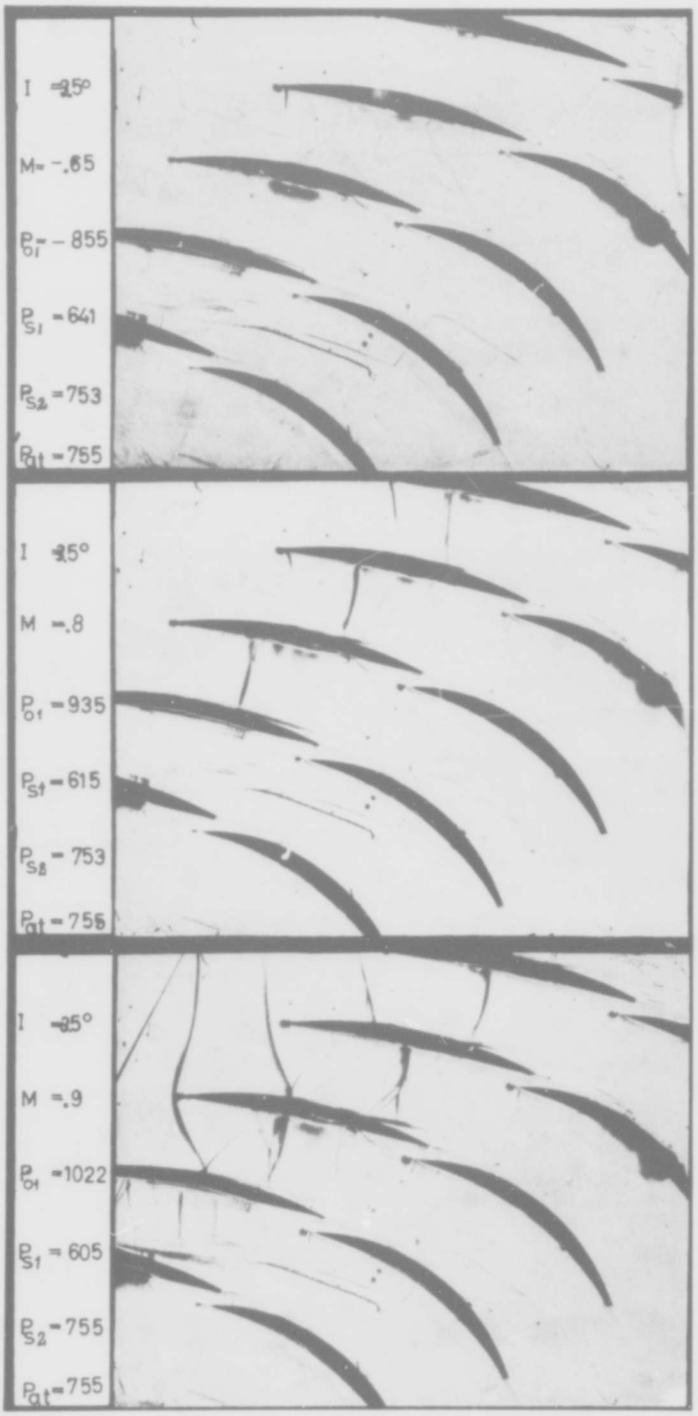

tandem cascade I

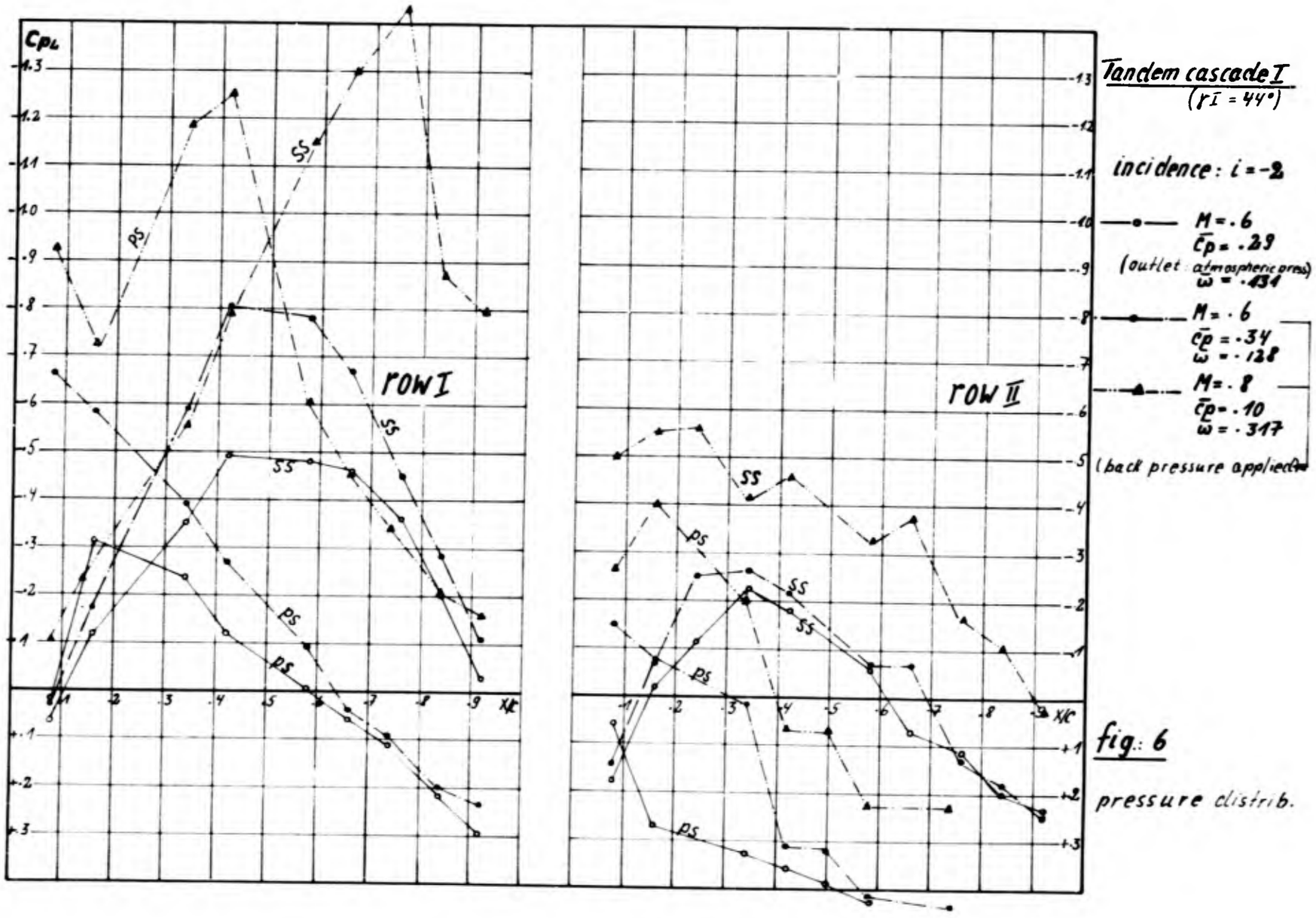

Tandem cascade I
($\gamma\bar{1} = 44°$)

incidence : $i = -2$

- M = .6, $\bar{C}p$ = .29, $\bar{\omega}$ = .434 (outlet atmospheric press)
- M = .6, $\bar{C}p$ = .34, $\bar{\omega}$ = .128
- M = .8, $\bar{C}p$ = .10, $\bar{\omega}$ = .317

(back pressure applied)

fig.: 6

pressure distrib.

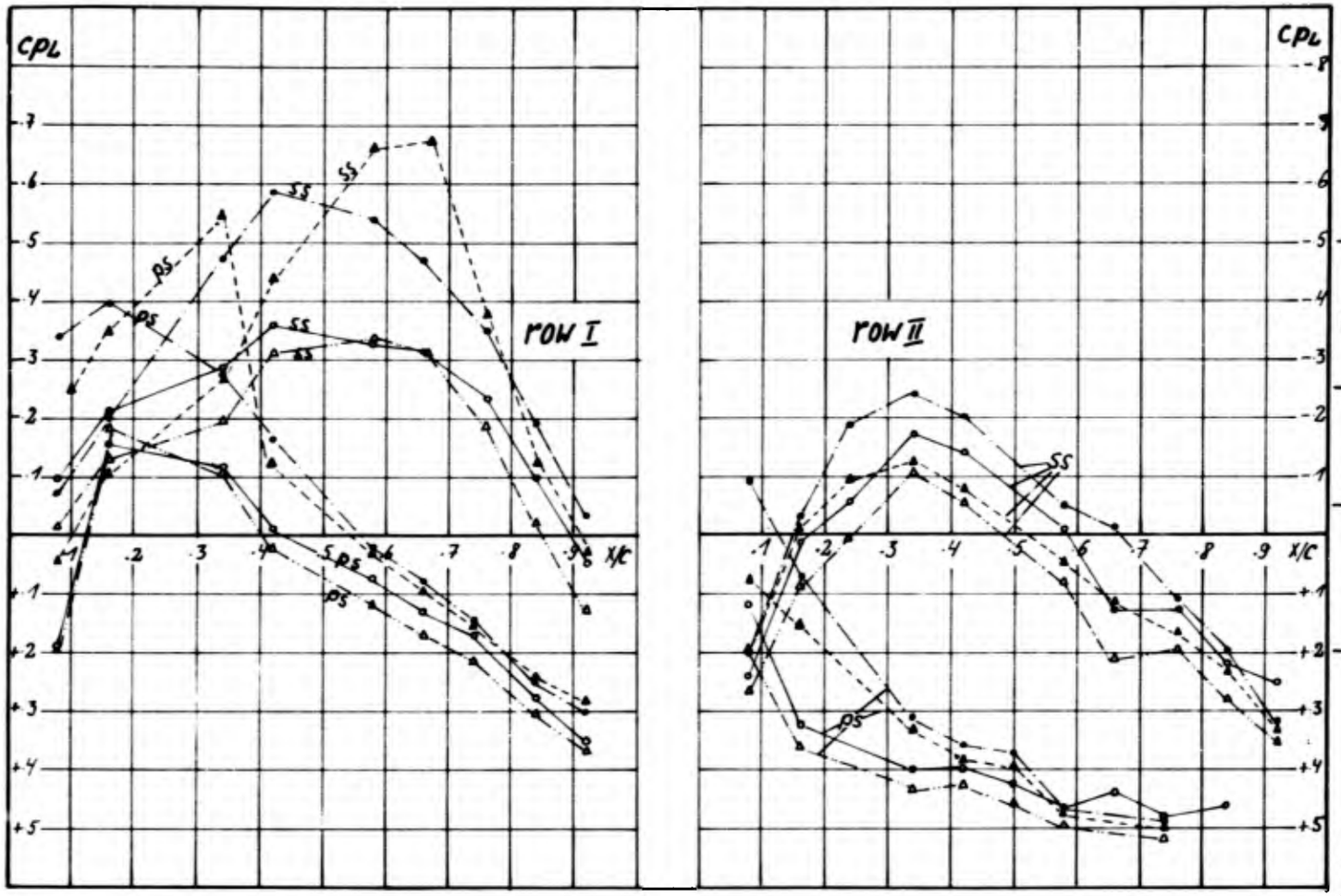

Tandem cascade I
($\gamma_I = 44°$)

incidence: $i = +2°$

— ● — $M = .6$
$\bar{c}p = .41$
$\bar{\omega} = .12$
(outlet atm. pressure)

— ● — $M = .6$
$\bar{c}p = .40$
$\bar{\omega} = .096$
(backpressure applied)

— ▲ — $M = .8$
$\bar{c}p = .38$
$\bar{\omega} = .127$
(outlet atm. pressure)

— ▲ — $M = .8$
$\bar{c}p = .41$
$\bar{\omega} = .147$
(backpressure applied)

fig.: 7

pressure distribution

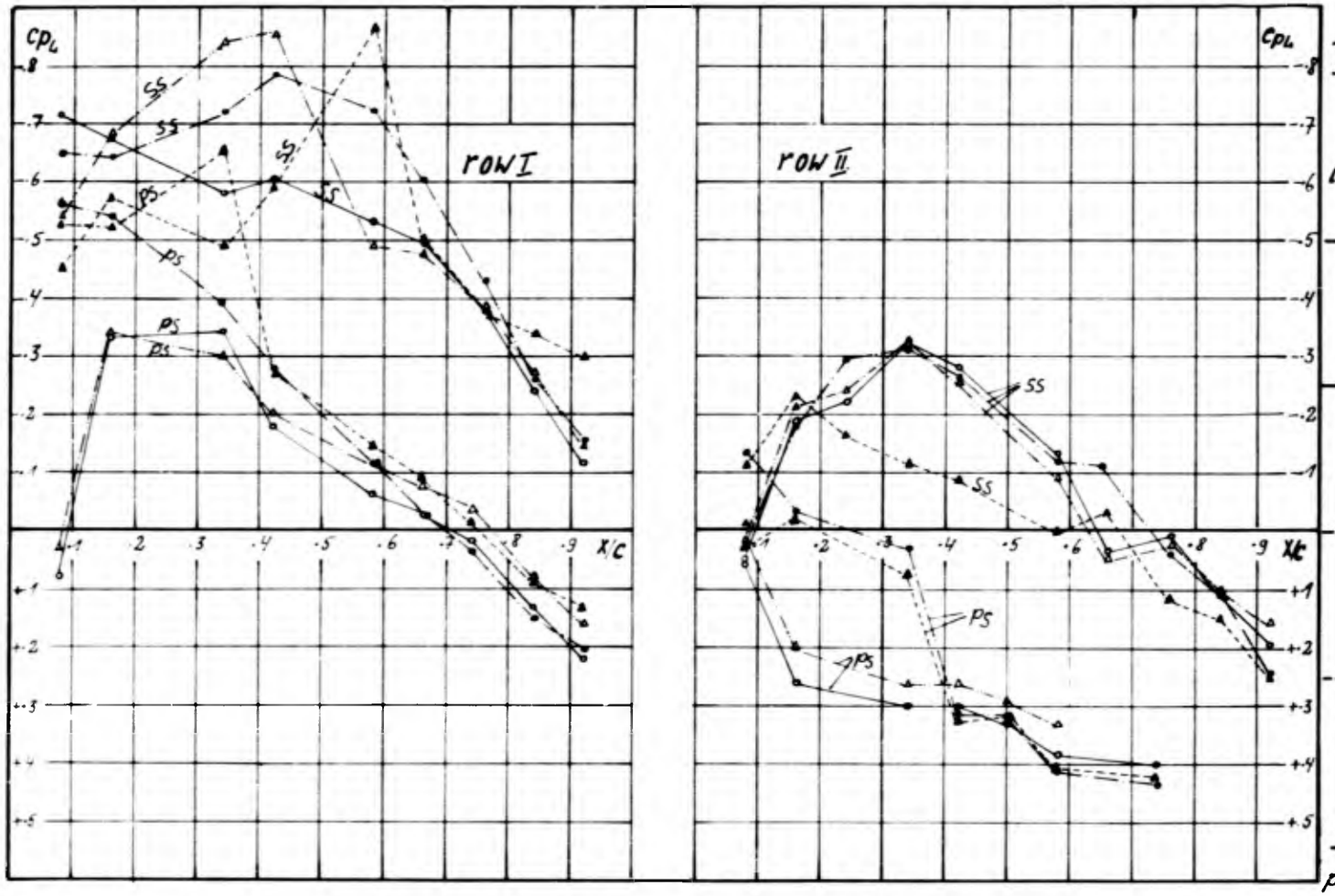

Tandem cascade I
($\gamma_I = 44°$)

incidence: $\bar{i} = +6°$

M = .6
$\bar{c}_p$ = .252
$\bar{\omega}$ = .193

M = .6
$\bar{c}_p$ = .308
$\bar{\omega}$ = .127

M = .8
$\bar{c}_p$ = .18
$\bar{\omega}$ = .335

M = .8
$\bar{c}_p$ = .298
$\bar{\omega}$ = .263

fig. 8

pressure distribution

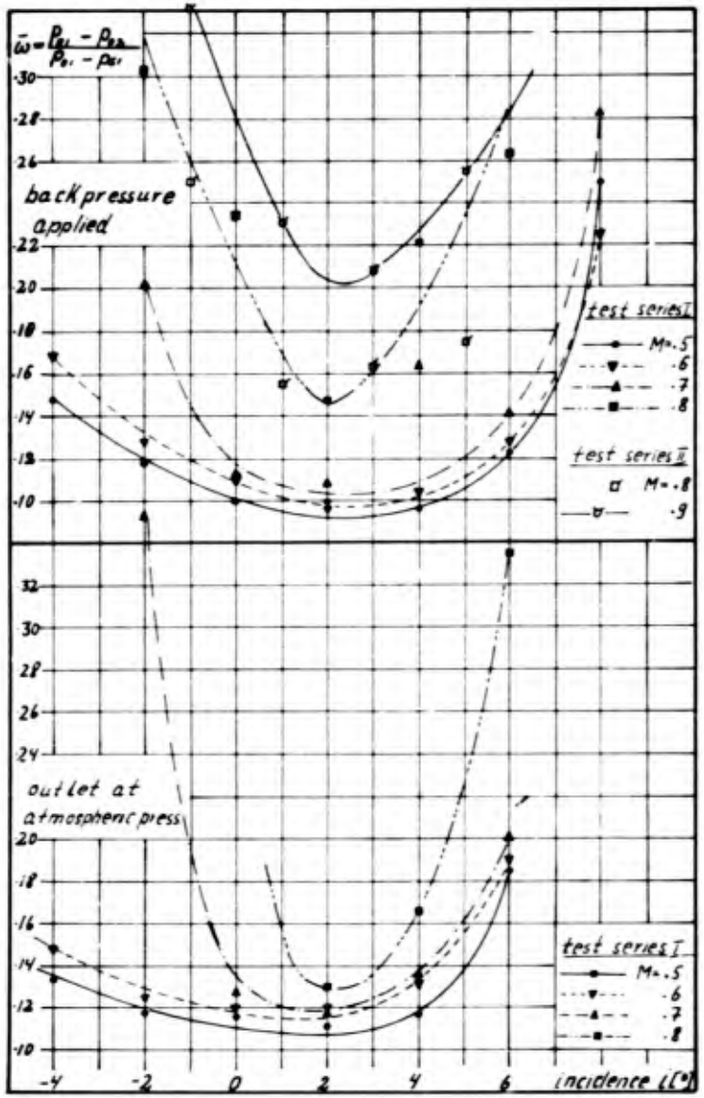

fig. 9a,b total pressure loss for tandem cascade I

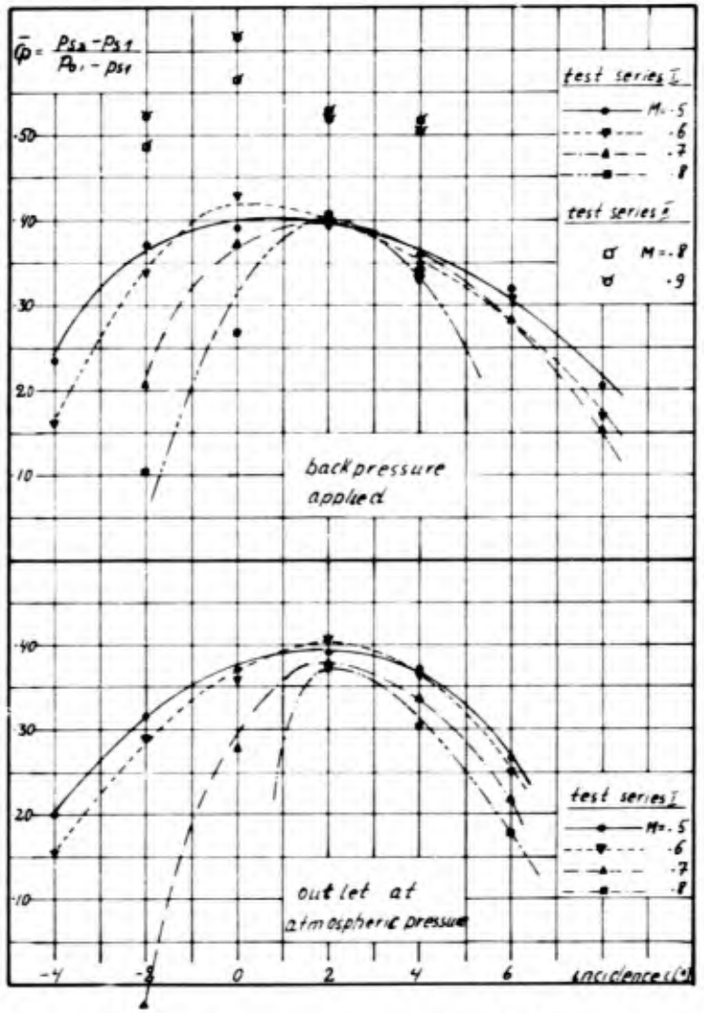

fig: 10a,b overall static pressure rise for tandem cascade I

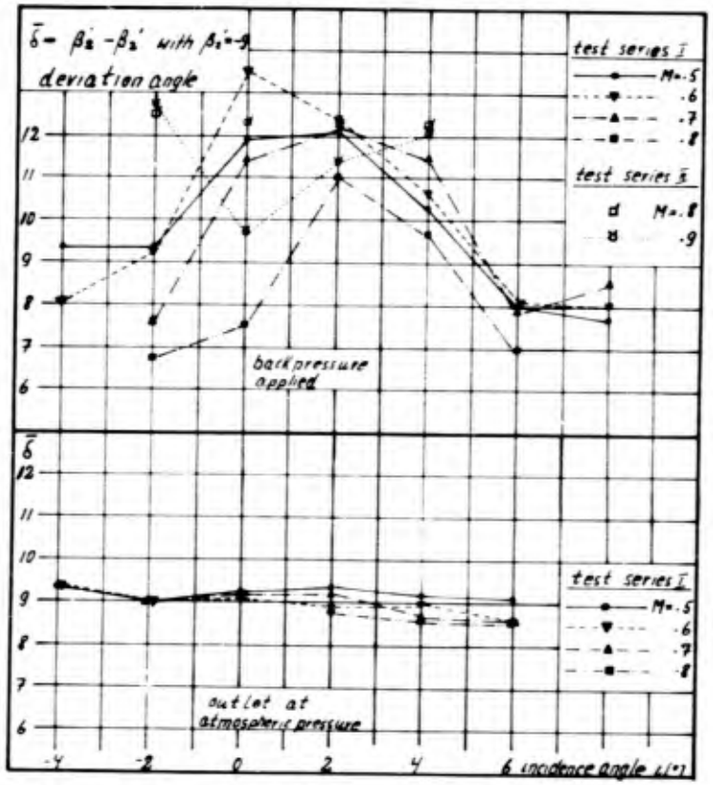

fig 11a,b deviation angle for tandem cascade I

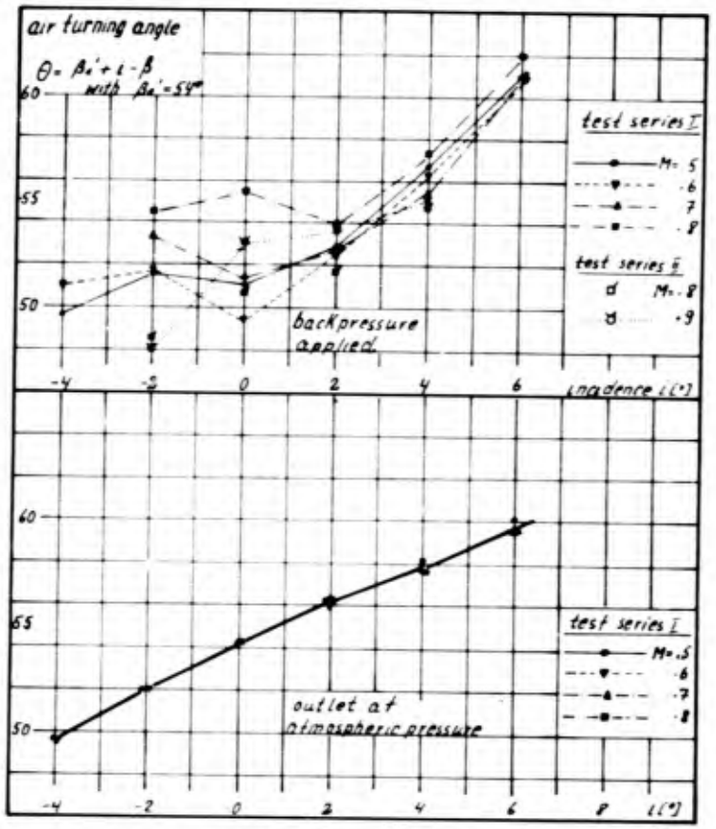

fig 12 a,b air turning angle for tandem cascade I

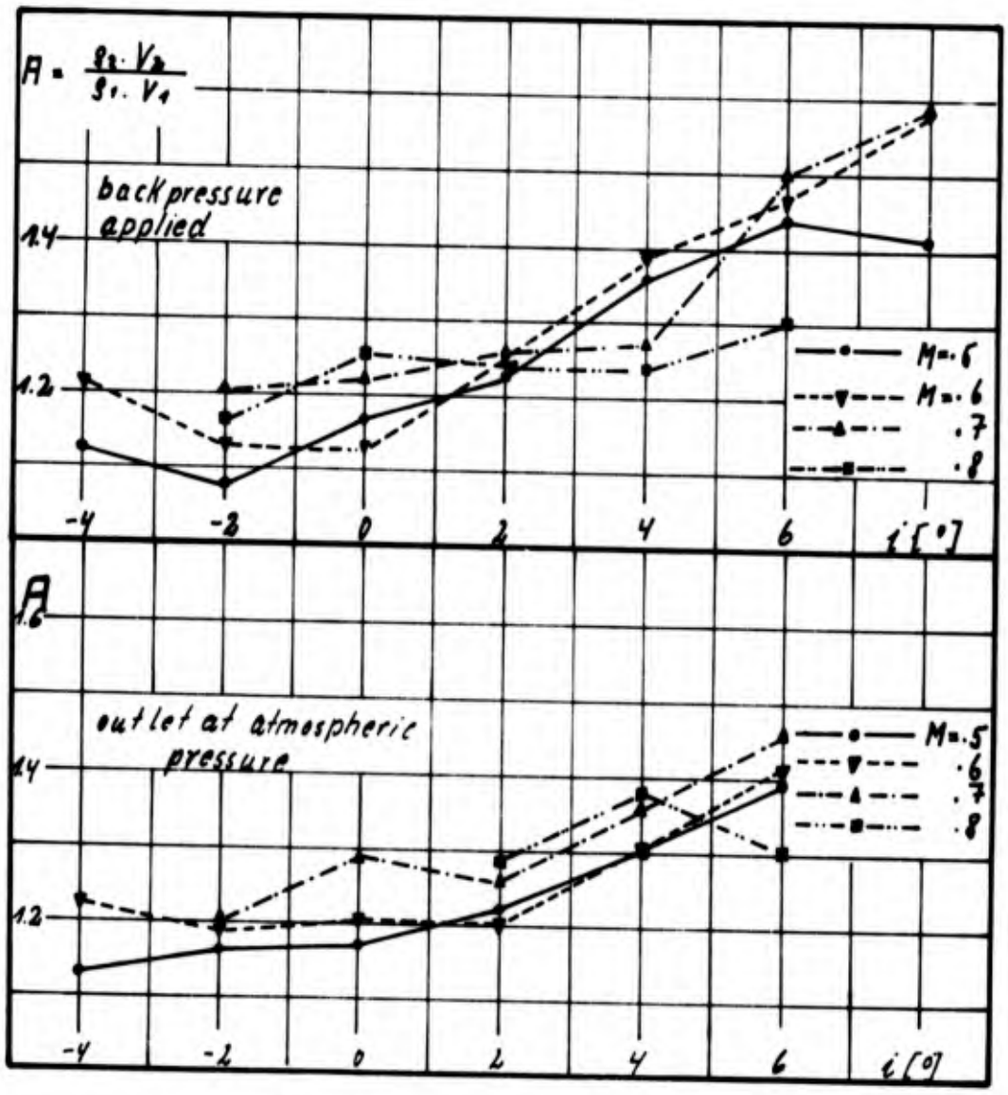

fig.: 13 a,b mass flow ratio for tandem cascade I

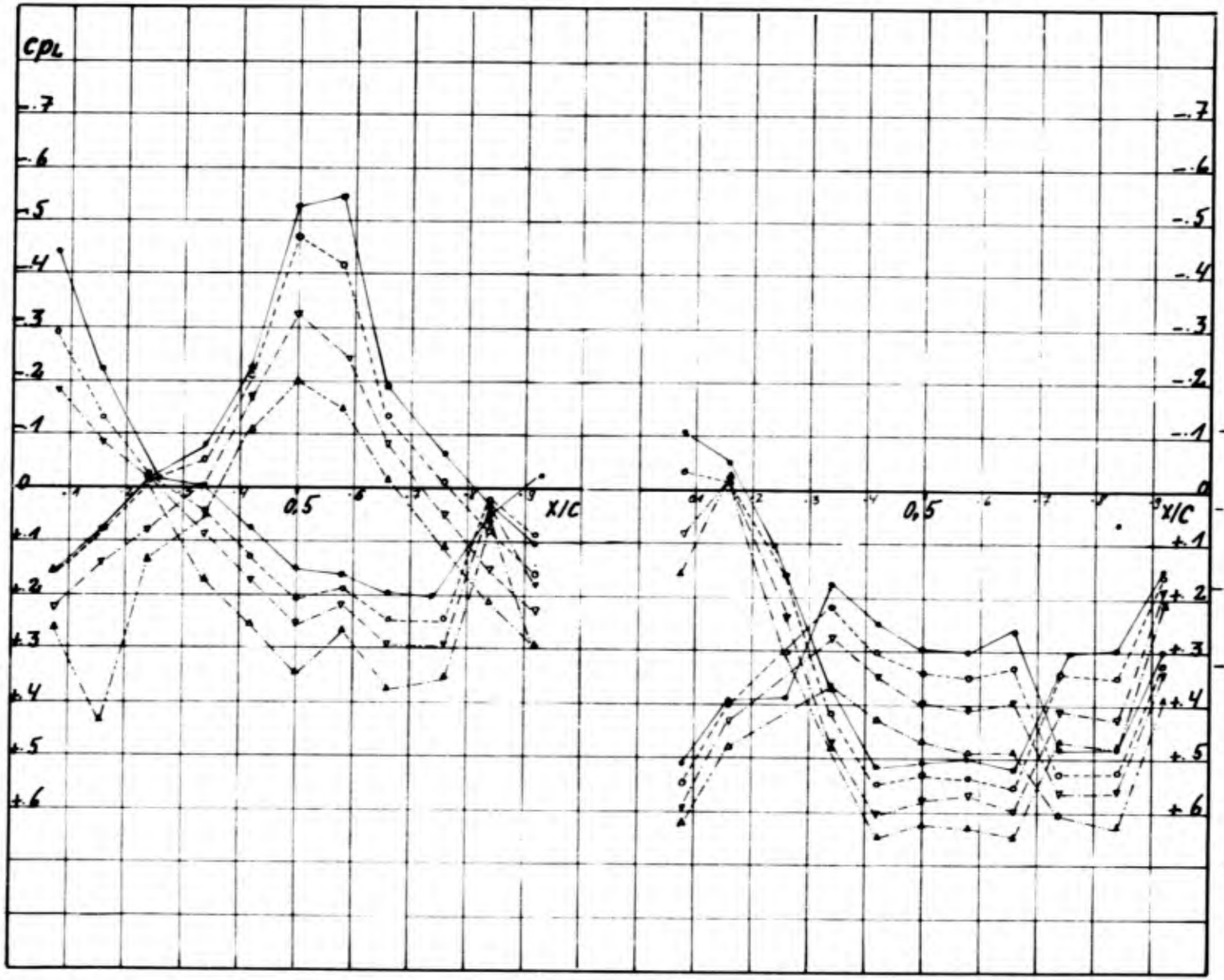

fig: 14

pressure distribution for cascade II

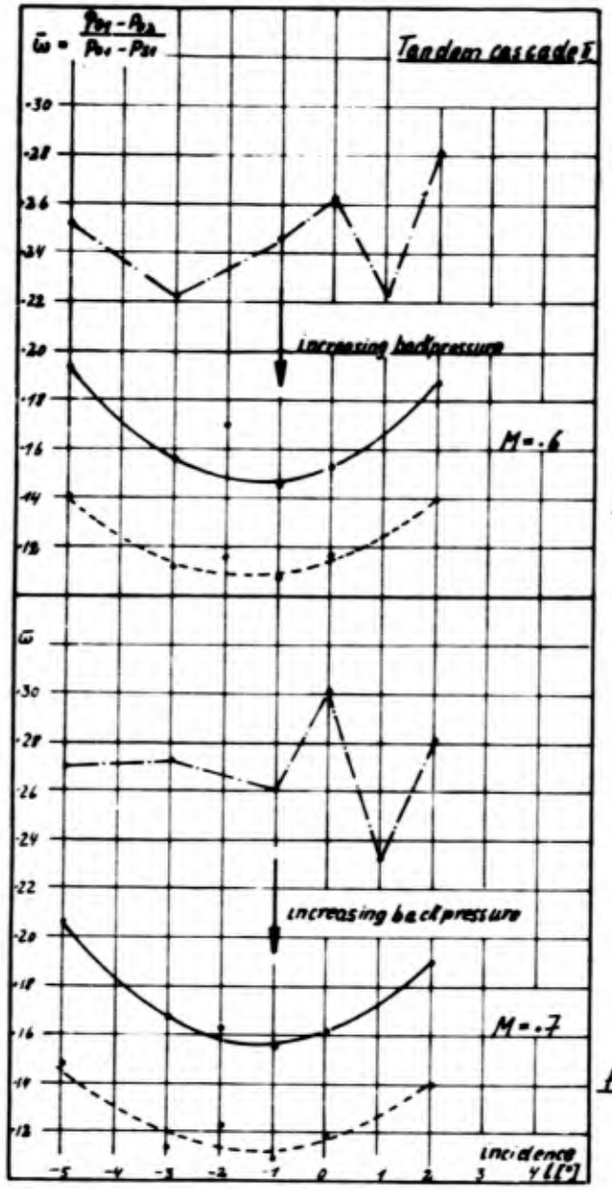

fig: 15a

fig: 15b

total pressure loss for tandem cascade I

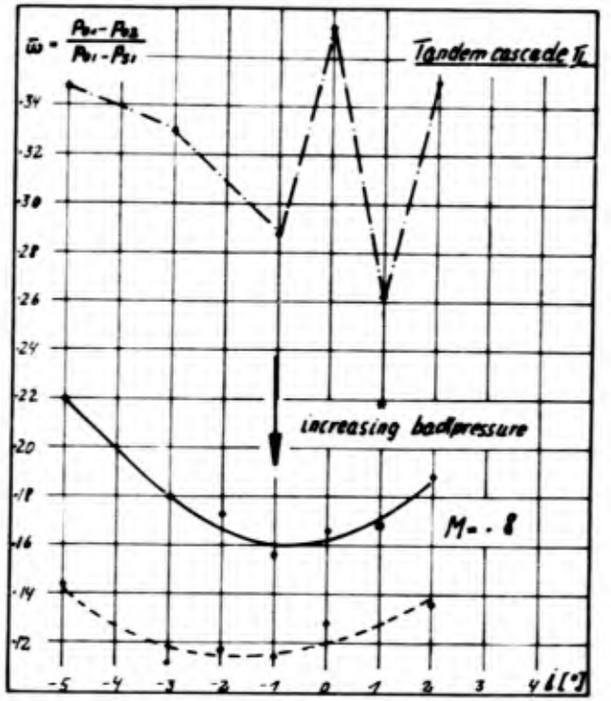

fig: 15c total pressure loss for tandem cascade II

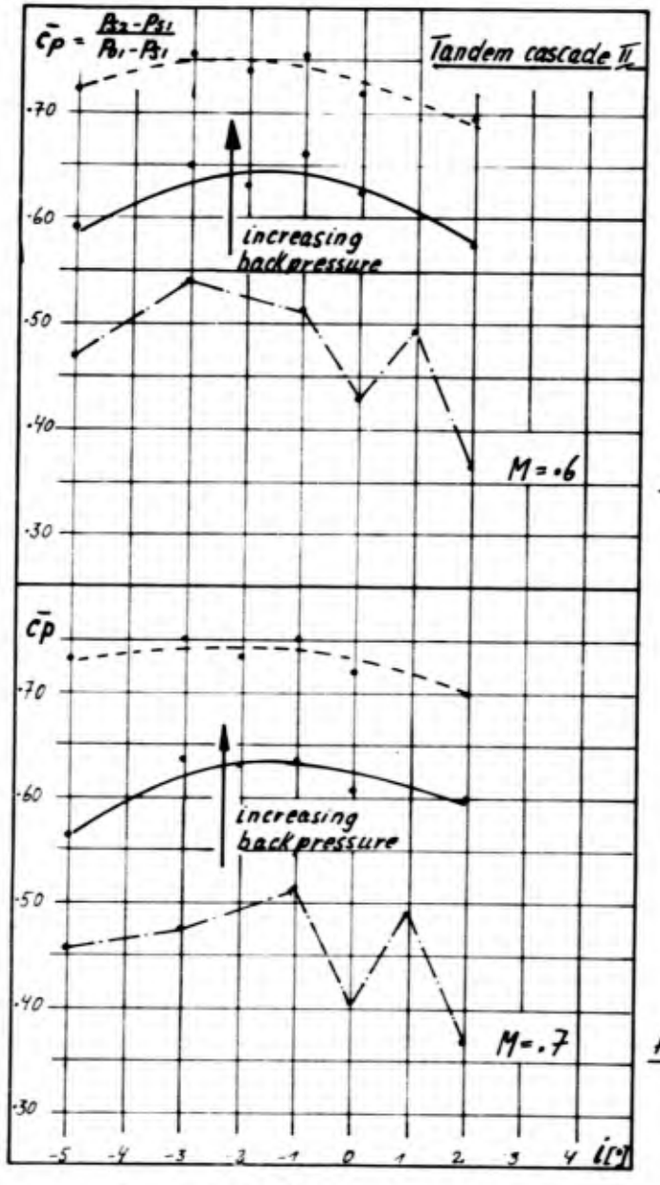

fig: 16a

fig: 16b

overall static pressure rise for tandem cascade II

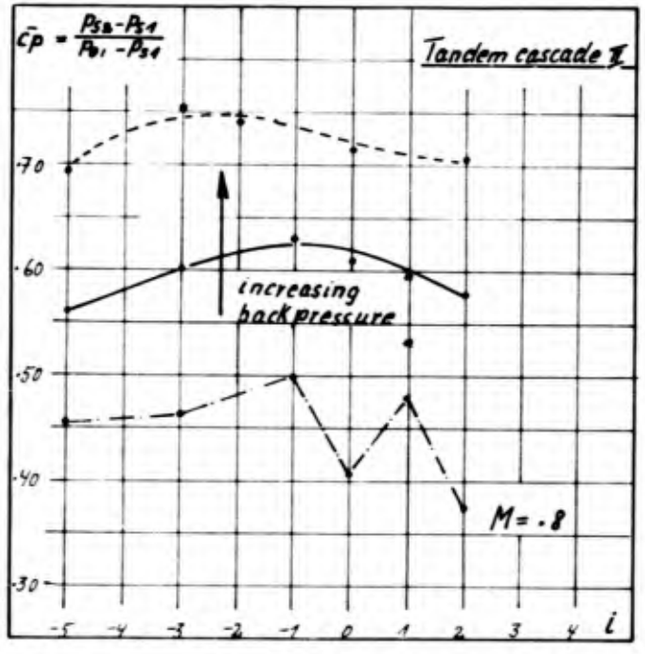

fig: 16c overall static pressure rise for tandem cascade II

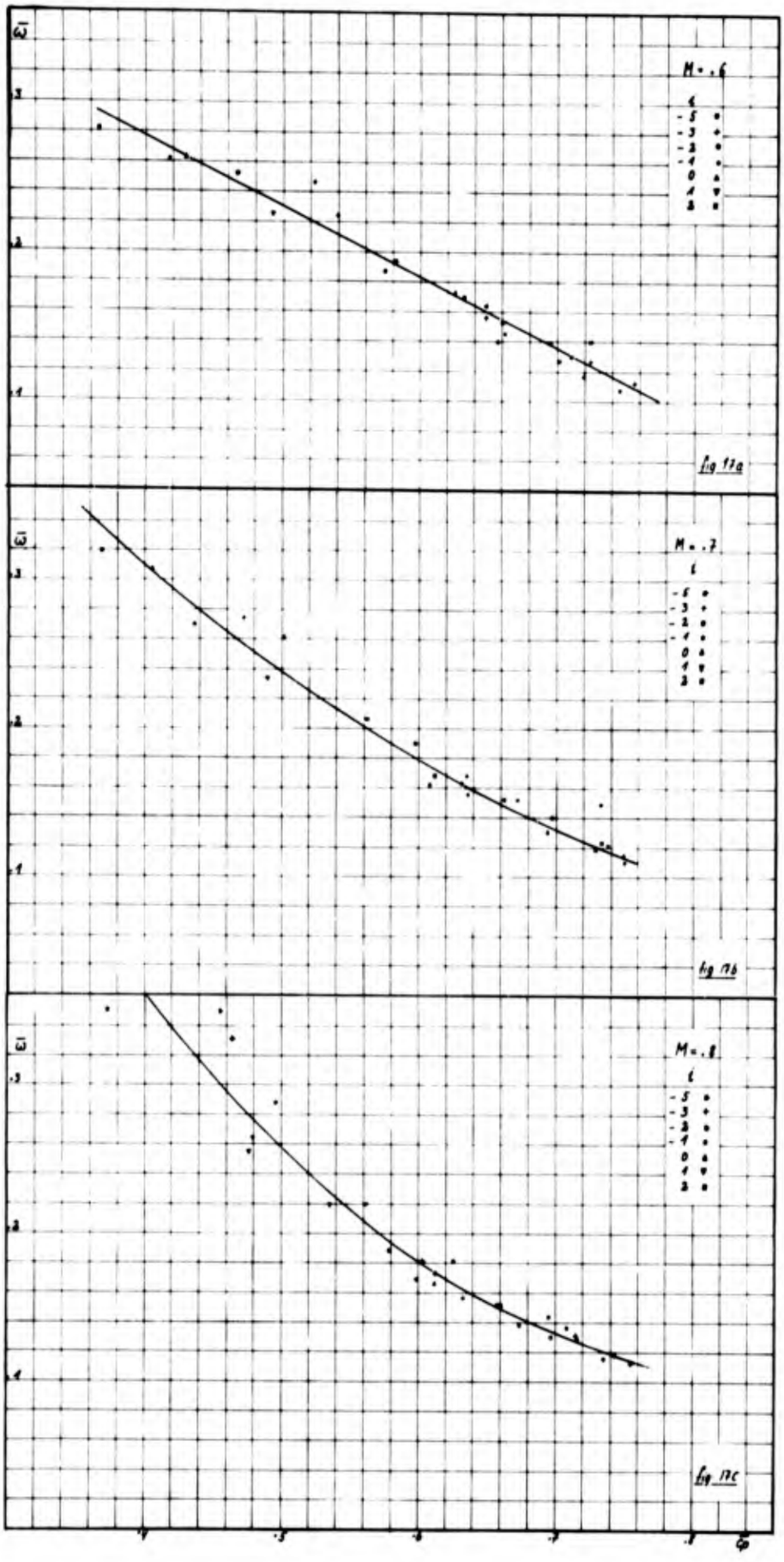
ω̄
M = .6
i
-5 o
-3 +
-2 ⊙
-1 ×
0 △
1 ▽
2 □
Fig 17a
ω̄
M = .7
i
-5 o
-3 +
-2 ⊙
-1 ×
0 △
1 ▽
2 □
Fig 17b
ω̄
M = .8
i
-5 o
-3 +
-2 ⊙
-1 ×
0 △
1 ▽
2 □
Fig 17c
Φ

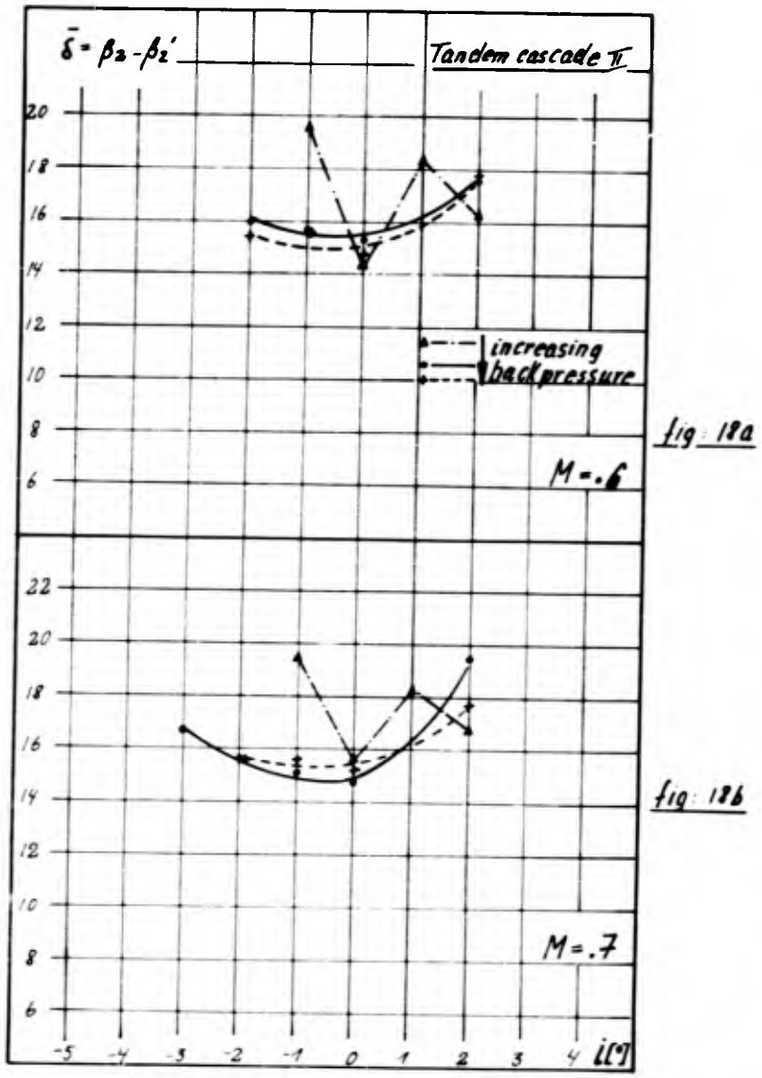

fig: 18a

fig: 18b

deviation angle for tandem cascade II

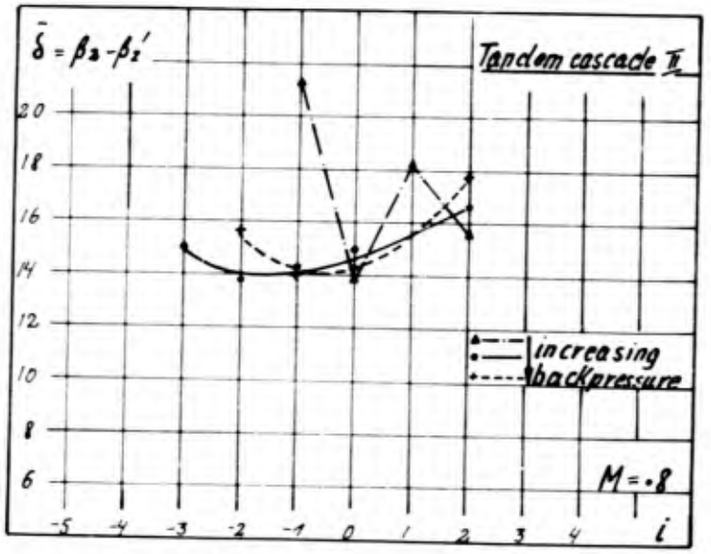

fig: 18c deviation angle for tandem cascade II

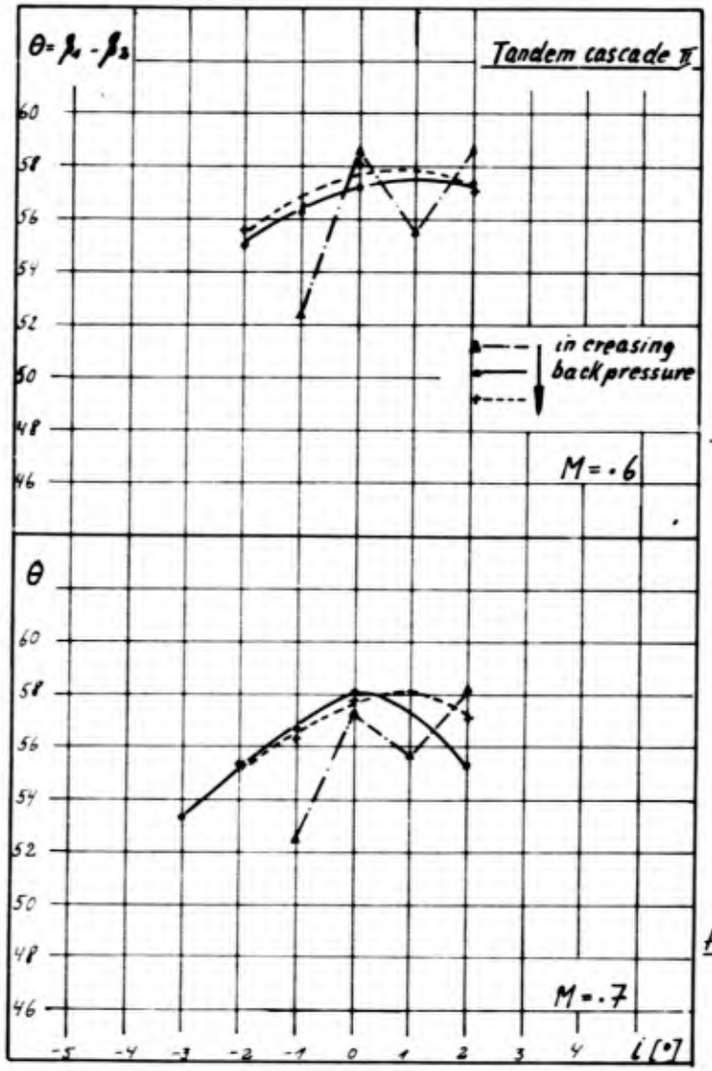

fig: 19a

fig: 19b

air turning angle for tandem cascade II

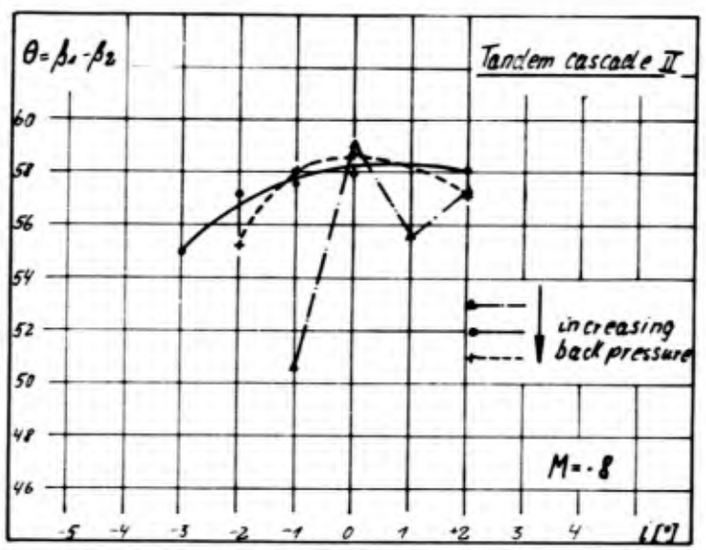

fig: 19c air turning angle for tandem cascade II